Journal of Alloys and Compounds 509 (2011) 8888–8893

Contents lists available at ScienceDirect

Journal of Alloys and Compounds

journal homepage: www.elsevier.com/locate/jallcom

Spectroellipsometric and photoluminescent studies of SnO_x nanostructures doped with Sm ions

V.G. Kravets*

Institute for Information Recording, NAS Ukraine, Kiev, Shpak Str. 2, 03113 Ukraine

ARTICLE INFO

Article history:
Received 17 April 2011
Received in revised form 20 May 2011
Accepted 23 May 2011
Available online 1 July 2011

Keywords:
Semiconductor nanoparticles
Rare earth photoluminescence
Optical characteristics
Ellipsometry

ABSTRACT

We present results on the photoluminescence and optical properties of SnO_x nanocrystals as a function of their size. Samariums ions are incorporated in SnO_x nanostructures to huge improve their photoluminescence efficiency. We have performed photoluminescent, ellipsometrical, atomic force microscopy, and structural studies of these nanocrystals and found them to be a direct semiconductor with a gap of ≈3.6 eV. The origin of the observed photoluminescence has been discussed. The doping of lanthanide atoms in semiconductor nanocrystals expands the range of possibilities offered by such materials, allowing them to be modified to meet specific requirements in electronic and optoelectronic applications.

1. Introduction

During the past two decades, the photoluminescence (PL) of semiconductor nanocrystals has been discussed intensively [1–3]. Investigation of the optical properties of semiconductor nanoparticles is important for both fundamental research and applications. Today, for example, semiconductors based on SnO_2 are the important materials for the microelectronics industry. SnO_2 is transparent semiconducting material with a tetragonal rutile structure and a wide band gap of around 3.6 eV and it is mainly used as gas sensors, transparent conductor, in photovoltaic cells, photocatalysis and optical materials [4]. Due to its large band gap and exciton binding energy, it is attractive as light emitters for the ultraviolet-visible spectral range. Nanostructures formed from wide band gap semiconductors are especially interesting and have potential use as luminescent materials in solid-state lighting [1,3]. For such applications, the oxygen vacancy related defect band can be used for down-conversion of excited UV or blue light into red region of the spectrum. Due to the reduction of the nonradiative contribution to the relaxation mechanism and the high photoluminescence efficiency because of a low cutoff vibrational energy (~600 cm^{-1}) the SnO_2 as a wide band gap semiconductor has huge attraction. Generally lanthanide ions such as Eu^{3+}, Er^{3+} and Sm^{3+}, etc., are incorporated in SnO_2 to improve the photoluminescence (PL) efficiency [3–5]. The luminescence in such structures is mainly due to the transitions of electrons between the spin-orbital splitted 4*f* states of the rare-earth atoms entering optical active centers. The ions of rare-earth elements incorporated in SnO_2 nanocrystals can also be selectively excited by energy transfer from the host matrix to the Eu^{3+}, Er^{3+} and Sm^{3+} ions. It was shown that the Eu^{3+} (or Sm^{3+}) emission can be strongly enhanced by energy transfer from the SnO_2 nanocrystals [3,5].

While SnO_2 pure nanostructures have attracted a lot of attention, the potential of such nanostructures activated by rare-earth Sm^{3+} ions has not been fully exploited yet. It is of great interest to distinguish between the luminescence arising from Sm^{3+} ions and of that arising from defect centers in the SnO_x matrix. Thus, the purpose of this paper is to study in detail the structural and the complex optical properties of SnO_x and SnO_x:Sm nanoparticles. The complex refractive index and absorption coefficient of the SnO_x-based nanostructures in the photon energy range of 1–5 eV have been determined with spectroscopic ellipsometry (SE). The results are discussed considering the effect of the nanocrystal size on the band gap altering. The dependences of the emissions originated from defects in SnO_x and Sm^{3+} ions in SnO_x:Sm on the SnO_2 nanocrystals size are found. The relation between the PL dependences and the absorption features has been confirmed. Our results demonstrated the strong influence on the PL spectra the absorption edge and additional states inside the band gap of SnO_2 semiconductor. The optical measurements have also provided evidence for a defect-related trap level that may be involved in the energy transfer between the SnO_x host and the Sm^{3+} ions.

2. Experimental details

We have fabricated two different versions of the SnO_x and SnO_x:Sm_2O_3 (5 wt%) nanoparticle samples: i) the powder; ii) the solutions of powder in the

* Tel.: +380 44454 2190; fax: +380 44454 2190.
E-mail addresses: vasyl_kravets@yahoo.com, vgk2007@ukr.net

0925-8388/$ – see front matter © 2011 Elsevier B.V. All rights reserved.
doi:10.1016/j.jallcom.2011.05.086

polymethyl-methacrylate (PMMA) and then spin-coated these solutions on top of the glass substrates resulting in a 130 nm thick film. The powder SnO_x particles were synthesized in a low pressure H_2/O_2/Ar premixed flame reactor. We have realized nanoparticles with sizes between 7 and 20 nm and oxygen stoichiometry of $x \approx 1.7$. For preparing the SnO_x:Sm_2O_3 powder we used following procedures: (i) mixing of SnO_x powder with 5 wt% Sm_2O_3; (ii) solution of SnO_x: Sm_2O_3 (5 wt%) in ethanol with adding of HCl acid by slow dropping; (iii) stirring of solution in ultrasound bath for 1 h; (iv) deposition of solution onto Si substrates; (v) drying of solution at room temperature. The final materials were also annealed in oxygen at 300 and 600 °C for 1 h. Such annealing helps to form samarium PL centers in SnO_x nanocrystals. For film-like specimens the SnO_x and SnO_x:Sm^{3+} powders were mixed with PMMA anisole solution. These mixtures were then spin-coated onto a glass slides to obtain about of 130 nm thick polymer films.

The structural characterization was done by atomic force microscopy (AFM) and X-ray diffraction (XRD) study. AFM analysis was performed in the tapping mode on the sample to examine the surface morphology in a scan area of 0.2 μm × 0.2 μm. XRD data were collected at 2θ angles ranging from 20° to 70° using Cu Kα radiation. A qualitative analysis included the phase identification.

The emission spectra of the photoluminescence were measured with a single beam spectrometer, in which two double diffraction monochromators were used. The PL was measured at room temperature in a back scattering geometry. The emission spectra were recorded using a CCD detector and corrected for the wavelength-depended sensitivity of the detection. The excitation was produced with a second-order Ti-sapphire CW laser λ = 400 nm (3.1 eV) and 488 nm line (2.54 eV) of an Ar^+ laser below the SnO_2 band gap (~3.6 eV).

To measure the optical response of the SnO_x and SnO_x:Sm^{3+} nanoparticles in polymer films we employed Woollam spectral ellipsometer in the 1.0–5.0 eV range at 60°, 65°, 70° incidence angles. The complex refractive index $n* = n + ik$ was directly determined from ellipsometric parameters $\psi(\lambda)$ and $\Delta(\lambda)$ [6]. The inversion of ellipsometric data was performed within the framework of film-substrate model (pure substrate was also measured). We take into account possible perturbations of the ellipsometric data due to surface roughness or grain texturing. Our measurements at multiple angles of incidence from 60° to 70° confirm that the surface roughness effect on $n* = n + ik$ is less than 5% over the measured spectral range and therefore does not significantly influence relative changes of $n* = n + ik$. From atomic force microscopy images the rms value of the surface roughness was found to be less than ~10 nm.

3. Results and discussion

AFM images of the SnO_x and SnO_x:Sm^{3+} films are shown in Fig. 1a and b. For structural analysis we have chosen the nanostructures after annealing at $T = 300$ °C for 1 h in pure O_2. Fresh SnO_x and SnO_x:Sm^{3+} nanoparticles have size about 10 nm. It was revealed that thermal annealing at $T = 300$ °C leads to an increase the diameter of nanocrystals by approximately ~10 nm and such treatment promotes to incorporate the atoms of Sm into crystal

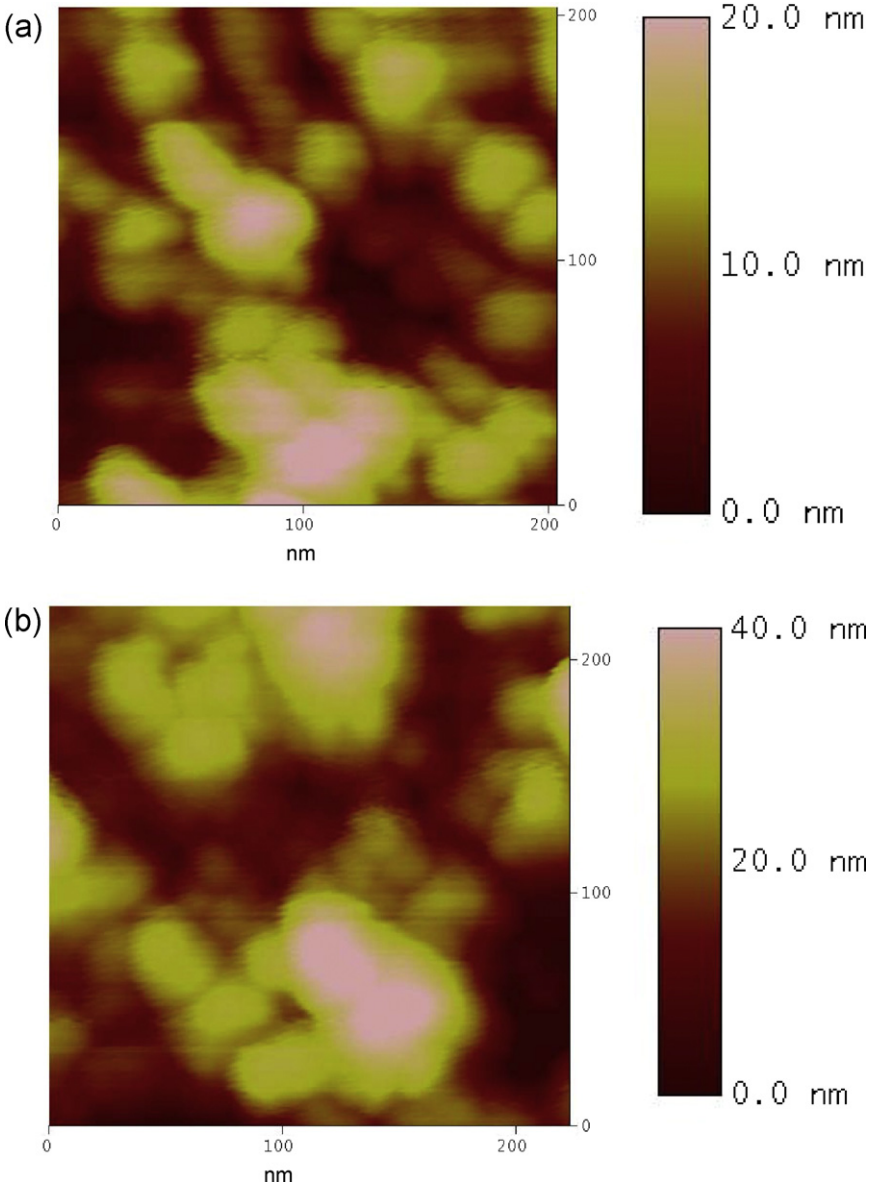

Fig. 1. AFM images of the SnO_x (a) and SnO_x:Sm^{3+} (b) nanostructures after their annealing at $T = 300$ °C for 1 h in pure O_2.

structure of Sn–O. It can be seen (Fig. 1a and b) that the particles form loosely agglomerated structures of fractal shape, consisting of nearly spherical primary particles. AFM witnesses the formation of the large number of SnO_x (Fig. 1a) and SnO_x:Sm^{3+} (Fig. 1b) clusters. The average particle size is about 20 nm. The AFM images of the nanoparticles show the existence of ordered SnO_2 cores and disordered (amorphous) shells. Note that the sizes of the SnO_x:Sm^{3+} particles are slightly larger than pure SnO_x.

The XRD spectra indicate a tetragonal SnO_2 phase in tin oxide nanoparticles. This phase is dominant with lattice constants $a \approx 4.75$ Å and $c \approx 3.19$ Å. Apart from the tetragonal phase we also reveal a low concentration of orthorhombic crystals. Doping of SnO_x nanocrystals with Sm atoms does not change the XRD spectra. Crystal lattice parameters are also not affected by the thermal treatment and for all samples the value is slightly higher in comparison to pure SnO_2. The diffraction peak (1 0 1) $2\theta = 39.63^\circ$ of the nanocrystalline film is broadened due to the small size of the crystals. Using the Sherrer formula [8] and the experimental width of this diffraction peak the average diameter of SnO_x was also determined. The XRD data confirm the average size of nanoparticles obtained from AFM measurements.

Fig. 2a shows the PL spectra of the SnO_x particles with different nanocrystal sizes. We started to measure the PL for fresh SnO_x particles ($D \sim 10$ nm), and then the size was increased due to annealing at $T = 300\,^\circ$C ($D \sim 20$ nm) and $T = 600\,^\circ$C ($D \sim 30$–35 nm). Annealing was done in pure O_2 during 1 h. There is a broad peak between 1.8 and 2 eV nm in the PL spectra for samples with $D = 10$ and 20 nm. No significant size dependence of the PL peak energy was observed. The highest PL efficiencies are observed for fresh sample with nanoparticle sizes about of 10 nm. Fig. 2a demonstrates that the annealing temperature has a strong effect on the PL intensity. The PL in red spectral region disappears after annealing of SnO_x nanocrystals at $T = 600\,^\circ$C for 1 h (Fig. 2a).

Strong photoluminescence in spectral region 1.8–2 eV for SnO_x nanoparticles can be caused by the presence of crystalline defects resulting from the synthesis process of nanostructures. With respect to the PL of the SnO_x nanoparticles, oxygen vacancies have been assumed to be the most likely candidates for the recombination centers in PL processes, which resemble that of other oxide nanocrystals such as ZnO, TiO_2, SiO_2 and Al_2O_3 [7–10]. Our experimental data confirm that the singly ionized oxygen vacancy can be responsible for the red emission in the SnO_x particles. This emission results from the recombination of a photogenerated hole with the singly ionized charge state of this defect. Additional thermal treatment these samples in O_2 air should be expected to decrease in the number of oxygen vacancies.

To find the physical origin of PL emission we should consider two kinds of defects, i.e., Sn vacancies (V_{Sn}) and oxygen vacancies (V_O) [11]. The oxygen defects create a defect band inside the band gap of pure SnO_2 which does not destroy the insulating behavior of SnO_2 but decreases its band gap (it was confirmed by measurements of absorption spectra, see below). This indicates that the O defect is electronic in nature. We can assumer that V_O are the recombination centers for the PL emission [12], which have an effective monovalent positive charge with respect to the regular O^{2-} site. Themlin et al. [12] based on data of synchrotron measurements of the SnO_2 (1 1 0) surface, suggested the existence of states sensitive to oxygen chemisorption, situated 1.4 eV above the valence band top. These levels related to the Sn^{2+} cation and associated with the presence of oxygen vacancies, are compatible with the electron transitions leading to the ~1.9 eV PL emission observed in the present work. The electron is promoted from the trapped band inside of band gap to the conduction band, leaving a hole in the trapped band. The active hole formed can be trapped at the V_O center directly to form the V_{OO} center. Thereafter, recombination of a V_{OO} center with a conduction band electron gives rise to the red

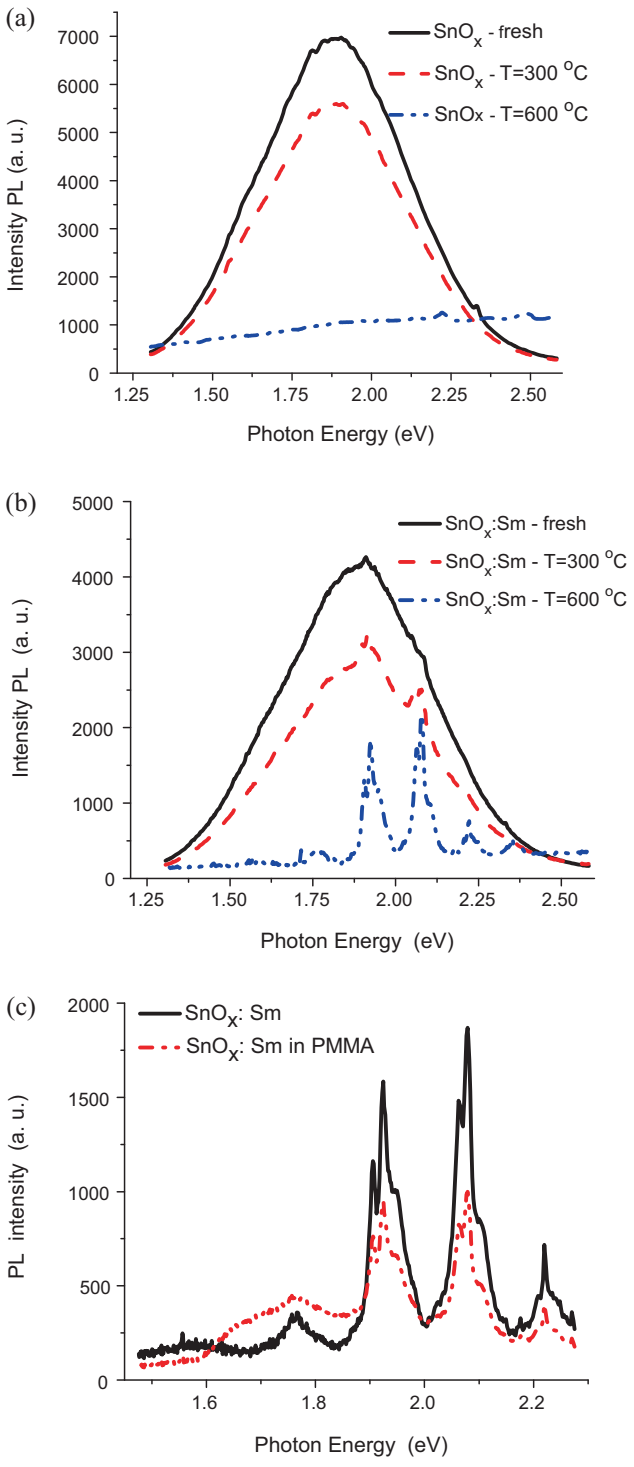

Fig. 2. Photoluminescence spectra of the SnO_x nanoparticles (a); PL spectra SnO_x:Sm^{3+} nanostructures for fresh ((intensity multiplied by ×10) and annealed at temperatures $T = 300\,^\circ$C (intensity multiplied by ×10) and at 600 °C 1 h in pure O_2 (b). Comparison the photoluminescence spectra of the SnO_x:Sm^{3+} powder nanocrystals and their solution in PMMA film (c).

photoemission. From the above scheme, it is clearly seen that the PL emission band has been generated due to the recombination of the trapped charges and photogenerated electrons from the conduction band. By annealing samples at low temperature ($T < 450\,^\circ$C) many more V_O centers are formed to maintain the balance of the valence compared with the initial condition. Subsequently, in the PL processes, more holes can be trapped at these V_O centers to form the

recombination center (V_{OO}) after photoexcitation of the SnO_2 nanoparticles. That is the reason the PL intensity becomes remarkably larger after annealing samples at $T = 300\,^{\circ}C$. The treatment of the sample under an oxygen atmosphere heated at $T = 600\,^{\circ}C$ causes the decrease of the PL emission in the red region. This experimental fact also indicates an annealing-induced decrease in the vacancy concentration due to the thermally activated oxygen diffusion.

Decreasing particle size has degraded the local symmetry of Sn–O bonds from D_{4h} to D_{3h} (V_h), which is the local structure of the optically active center that gives strong PL [11,12]. Oxygen vacancies are the postulated main source of electron states on the surface of particle. The ratio between surface states and bulk electron states decreases while the particle size increases. Therefore, the efficiency of absorbance in the region of 400–550 nm (or PL emission in 600–650 nm) rises with decreasing particle size.

By incorporating Sm^{3+} ions into the SnO_2 host lattice, many more V_O centers are formed to maintain the balance of the valence compared with the initial condition. Fig. 2b shows evolution of the PL spectra for SnO_x:Sm^{3+} nanoparticles before and after their annealing at $T = 300\,^{\circ}C$ and $T = 600\,^{\circ}C$ for 1 h in pure O_2. The PL spectra of fresh SnO_x:Sm^{3+} demonstrate a wide band (Fig. 2b), which is located in the red spectral region and its spectral dependence is closed to those of pure SnO_x nanoparticles (Fig. 2a). After first step annealing at $T = 300\,^{\circ}C$ this sample exhibits the strongest red PL which can be seen by eyes (in Fig. 2b, intensity of PL gives in relative units for best demonstration of the spectral changes in PL spectra). Note that the shape of PL dependences shows the appearance of emission lines. These lines stay stronger after annealing the SnO_x:Sm^{3+} nanostructures at $T = 600\,^{\circ}C$ for 1 h. Note that at 400 nm excitation the SnO_x:Sm^{3+} samples annealed at 600 °C show one order of magnitude higher luminescence efficiency in comparison to fresh SnO_x nanoparticles (Fig. 2a).

There are several sharp peaks between 1.6 and 2.4 eV in the PL spectra of annealed SnO_x:Sm^{3+} sample. The peaks at ~1.77, ~1.92, ~2.08 and ~2.21 eV could be attributed to the $^4G_{7/2,5/2} \rightarrow {}^7H_{n/2}$ ($n = 3$, 5 and 7) transitions of Sm^{3+} [13–15], because these intracentre transitions in the Sm^{3+} ions place for materials activated rare-earth ions. The Sm^{3+} ions can create the electron states in the bandgap of wide-gap semiconductors [1,3,13]. Such kinds of states were observed in the electron spectra of Y_2O_3 and CeO_2 nanocrystals doped with Eu and Sm [13–15]. In these nanostructures the visible emission of trivalent samarium Sm^{3+} consists of transitions from the $^4G_{5/2}$ excited state to the lower ^6H_j ($j = 5/2$, 7/2, 9/2 and 11/2) energy levels. In our case the visible emission spectra of SnO_x:Sm^{3+} nanocrystals (Fig. 2b and c) following excitation with 400 nm (3.1 eV) and 488 nm (2.54 eV), are dominated by the transitions $^4G_{5/2} \rightarrow {}^6H_{7/2}$ at approximately 2.08 eV. Additional strong emissions were observed at 1.92 and 1.77 eV and can be associated with the $^4G_{5/2} \rightarrow {}^6H_{5/2}$ and $^4G_{5/2} \rightarrow {}^6H_{9/2}$ transitions, respectively. Note that the SnO_x:Sm^{3+} nanocrystals soluble in PMMA matrix and performed in polymer films show also a visually dominant red emission due to the $^4G_{5/2} \rightarrow {}^6H_{7/2}$ electron transitions (Fig. 2c). The spectral dependence of the PL is not significantly changed for filmed solution of SnO_x:Sm^{3+} in PMMA. Therefore, the spectral structure of PL shown in Fig. 2b and c indicates that Sm^{3+} can indeed be doped in SnO_x nanocrystals. The sudden increase in PL emission output after annealing at 600 °C is believed to be caused by the decrease defector dopant-related non-radiative relaxation cannels for excited Sm^{3+} ions.

With the aim to persuade that the introducing of the Sm^{3+} ions into SnO_x nanocrystals leads to form additional electronic states inside of the band gap we have performed the measurement and comparison of the complex refractive index for the SnO_x and SnO_x:Sm^{3+} films. Such investigations allow determining the influence of the confinement (size) effect on the energy spectra of nanocrystals. To extract the effective refractive index of

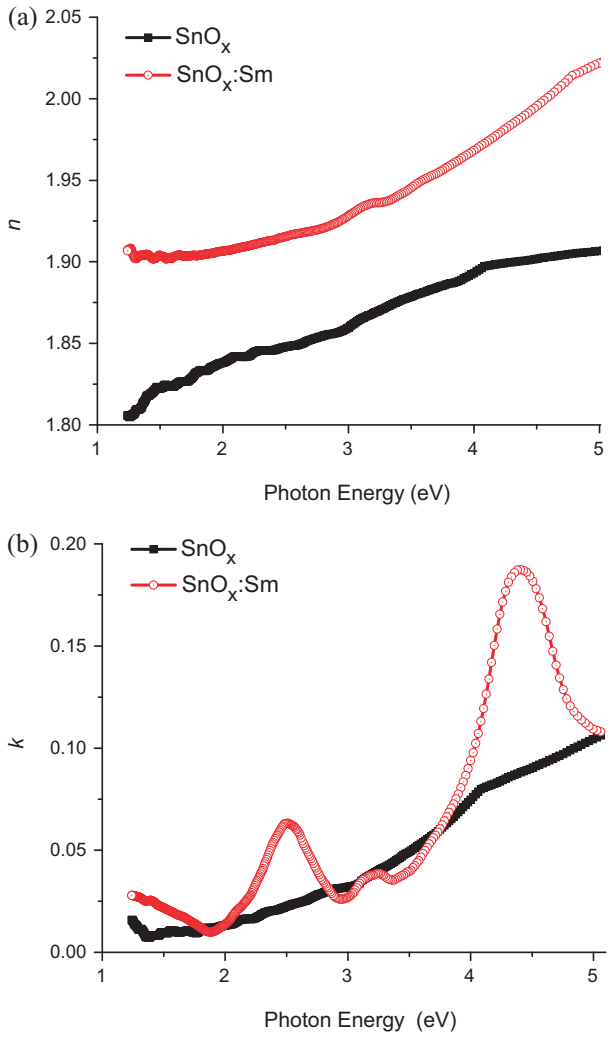

Fig. 3. Optical properties of the SnO_x and SnO_x:Sm^{3+} nanostructures: the real (a) and imaginary (b) parts of the effective refractive index.

the studied nanocomposites we use the Maxwell-Garnet effective medium approximation (EMA) [16,17]. EMA describes the interaction between the incident light and nanostructured materials and assigns a complex effective index of refraction to such structures.

The effective complex dielectric function, ε_e, for a composite system containing semiconductor nanoparticles embedded in a host dielectric matrix is defined by relationship [16,17]:

$$\varepsilon_e = \varepsilon_d \frac{\varepsilon_m(1+2x) + 2\varepsilon_d(1-x)}{\varepsilon_m(1-x) + \varepsilon_d(2+x)}, \quad (1)$$

where ε_e, ε_d, and ε are the effective complex dielectric functions of polymer film, dielectric (PMMA) and SnO_x (SnO_x:Sm^{3+}) nanocrystals, respectively; x is a particle volumetric concentration in film. The optical constants of a PMMA film have been parameterized by the Cauchy function. To find Cauchy coefficients we again carried out spectroscopic ellipsometry measurements of pure PMMA film.

Fig. 3a and b shows the extracted optical constants n and k ($n + ik = \sqrt{\varepsilon}$) for SnO_x and SnO_x:Sm^{3+} nanocrystals. These figures display the complex refractive index for samples annealed at 600 °C, when the influence of defect states in the band gap of SnO_x is minimized and Sm^{3+} ions can create additional energy levels (as was assumed from PL data). The values of n for SnO_x:Sm^{3+} nanocrystals are slightly larger than those of SnO_x (Fig. 3a) and these data are consistent with reported in literature [18] for SnO_2 films. We also see that the real part of the refractive index, n, increases with the

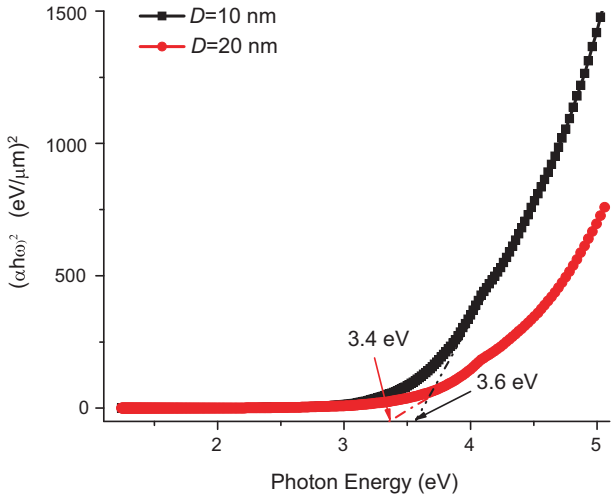

Fig. 4. Experimental absorption spectra for the SnO_x nanocrystals plotted as $(\alpha\hbar\omega)^2$.

increase of photon energy. The values of n ranged from 1.8 to 2.05 and they are slightly smaller than that of bulk SnO_2.

The imaginary part of the refractive index k increases with increasing of the photon energy in case of SnO_x nanocrystals (Fig. 3b). It is clear seen the existence of the weakly absorbed region (values of k is small for photon energy $E < 3$ eV) and strong absorbance region 3–5 eV. Such dependence of k confirms the sharp interband absorption edge around photon energy 3.4–3.6 eV.

Three pronounced extinction peaks appear in k dependence for SnO_x:Sm^{3+} nanocrystals, (see Fig. 3b). These absorption peaks are located at $\hbar\omega \sim 2.5$, ~3.2 and ~4.4 eV. The energy position of these peaks for different annealing temperatures does not change. The broad absorption bands at $\hbar\omega \sim 2.5$, ~3.2 eV are correlated to the f–f transitions of Sm^{3+} ions due to splitting these levels in crystal field of host (SnO_x). Such tendency in extinction spectra of SnO_x:Sm^{3+} nanocrystals confirms the suggestion that samarium ions can introduce additional energy levels in the forbidden gap of SnO_x semiconductor. Therefore, the absorption in SnO_x:Sm^{3+} nanocrystal is a sum of absorption at edge of band gap in SnO_x semiconductor and the electron transitions between the individual energy levels of Sm^{3+} ions. Moreover, the absorption peak in k at $\hbar\omega \sim 3$–3.2 eV coincides with the exciting energy of laser $\lambda \approx 400$ nm (3.1 eV) which is used for stimulating of PL. To summarize, the emission lines in PL spectra (Fig. 2b and c) and broad maxima in extinction spectra (Fig. 3b) are results of the transitions of electrons between the energy levels of Sm^{3+} ions which are splitted by the crystal field of SnO_x nanocrystals. The broad UV peak in k at $\hbar\omega \sim 4$ eV is also the direct Sm^{3+} ions excitation peaks. According to Ref. [19], Sm^{3+} ions produce ^4L_j energy levels, close to bottom of E_g. The absorption can occur at high-energy excitation ($E > 4$ eV), because the electrons may go from one of these energy levels to conduction band of the SnO_2 semiconductor. Moreover, an efficient energy transfer from the SnO_2 host to the Sm^{3+} ions can take place. Due to this the excitation efficiency is much higher for the Sm^{3+} ions in the nanocrystals of SnO_x by energy transfer from the SnO_x host.

Finally, we consider the dependence of absorption spectra ($\alpha = 4\pi k/\lambda$) of the SnO_x particles on the particle sizes. The measurements of the UV–vis absorption spectra show that the absorption of the SnO_x particles (Fig. 4) is dominated by the band-edge, which associated with the interband electronic transitions. To determine the transition type and band gap E_g (the absorption edge), we fit the curve with the direct transition equation of $\alpha(\hbar\omega) = (\hbar\omega - E_g)^{1/2}/\omega$. These spectra show a blueshift of the absorption edge while the particle size decreases from 20 to 10 nm. We find the curve $\alpha(\hbar\omega)$ reveals direct absorption edge with the E_g to be about 3.6 eV for particles with $D = 10$ nm. So it is quite evident that the optical band gap of SnO_x ($x \approx 1.7$) nanocrystal is closed to the band gap of bulk SnO_2. The reduction of band gap energy for SnO_x particles with $D = 20$ nm is due to significant disorder and changes in the SnO_2 structure. This is also supported by Urbach tail states due to nonzero electronic densities of states close to the band edges.

It should be taken into account that the efficiency of absorbance in the region of 400–550 nm decreases with increasing particle size. This result shows that the intensity of PL is well correlated with the absorption of light by the SnO_x nanocrystallites. Consideration of this effect is expected to rise the PL intensity for fresh samples (with $D = 10$ nm), which posses the strongest absorption. The PL spectra obtained for different excitation wavelengths ($\lambda = 400$ and 488 nm) show that the spectral variation of the PL is almost independent of the excitation energy, provided it is lower than the band gap of the material. Moreover, the incorporation of Sm^{3+} ions in SnO_x nanocrystal sufficiently modifies the absorption and emission properties of wide gap SnO_x semiconductor in blue-green region. The emission and absorption of Sm^{3+} ions consists of several strong bands which are associated with the electron transitions between $^4G_{5/2}$ excited state and $^6H_{5/2}$ and $^6H_{7/2}$ base states. The 2.08 eV emission observed in SnO_x:Sm^{3+} seems to belong to the spin-orbital splitted 4f states transitions. With respect to the prominent emission centered at 1.9 eV, which can be attributed to electron transition mediated by defects levels in the band gap of pure SnO_x, such as oxygen vacancies, the intensity of PL at 2.08 eV in SnO_x:Sm^{3+} crystal has been enhanced many orders of magnitude than that of pure SnO_x due to the addition of the Sm^{3+} dopant.

4. Conclusions

The photoluminescence spectra of the pure wide gap SnO_x semiconductors and Sm^{3+} ion doped in SnO_x nanocrystals were investigated. It was shown that the photoluminescence spectra of the tin-oxide nanocrystals characterize a band at ~1.9 eV, which is associated with oxygen vacancies. Electronic properties of SnO_x and SnO_x:Sm^{3+} nanoparticles were investigated by measuring ellipsometric characteristics. It was revealed the existence of the new absorption peaks in the band gap of SnO_x:Sm^{3+} which is caused by the transitions of electrons between the spin-orbital splitted 4f states of the rare-earth atoms. Such additional absorption of the light in SnO_x:Sm^{3+} nanocrystal stimulates the increase of the intensity of PL in the red region up to two orders in comparison to the defect imitated emission in SnO_x nanocrystals. It was shown the blueshift of the absorption edge for SnO_x nanoparticles while the particle size decreases from 20 to 10 nm.

References

[1] S.V. Gaponenko, Optical Properties of Semiconductor Nanocrystals, Cambridge University Press, Cambidge, 1998.
[2] C. Delerue, G. Allan, M. Lannoo, Phys. Rev. B 48 (1993) 11024.
[3] V.G. Kravets, Opt. Spectrosc. 103 (5) (2007) 766–771.
[4] E.E. Nyein, U. Hommerich, J. Heikenfeld, D.S. Lee, A.J. Steckl, J.M. Zavada, Appl. Phys. Lett. 82 (2003) 1655–1657.
[5] R.S. Ningthoujam, V. Sudarsan, S.V. Godbole, L. Kienle, S.K. Kulshreshtha, A.K. Tyagi, Appl. Phys. Lett. 90 (2007) 173113.
[6] R.M.A. Azzam, N.M. Bashara, Ellipsometry and Polarized Light, North Holland Press, Amsterdam, 1987.
[7] N.E. Hsu, W.K. Hung, Y.F. Chen, J. Appl. Phys. 96 (8) (2004) 4671–4673.
[8] K. Vanheusden, W.L. Warren, C.H. Seager, D.R. Tallant, J.A. Voigt, B.E. Gnade, J. Appl. Phys. 79 (10) (1996) 7983–7990.
[9] F. Huisken, B. Kohn, V. Paillard, Appl. Phys. Lett. 74 (25) (1999) 3776–3778.
[10] X.S. Fang, C.H. Ye, X.X. Xu, T. Xie, Yu.C. Wu, L.D. Zhang, J. Phys.: Condens. Matter 16 (2004) 4157–4163.
[11] G. Rahman, V.M. Garcia-Suarez, S.C. Hong, Phys. Rev. B 78 (2008) 184404.
[12] J.M. Themlin, R. Sporken, J. Darville, R. Caudano, J.M. Gilles, R.L. Johnson, Phys. Rev. B 42 (18) (1990) 11914–11925.

[13] V.G. Kravets, J. Opt. Mater. 16 (2001) 369–375.
[14] F. Vetrone, J.-C. Boyer, J.C. Capobianco, et al., Nanotechnology 15 (2004) 75–79.
[15] Sh. Fujihara, M. Oikawa, J. Appl. Phys. 95 (12) (2004) 8002–8005.
[16] J.C. Maxwell-Garnett, Philos. Trans. R. Soc. London, Ser. A 203 (1904) 385.
[17] D. Stroud, Phys. Rev. B 12 (1975) 3368–3373.
[18] S. Goldsmith, E. Cetinorgu, R.L. Boxman, Thin Solid Films 517 (2009) 5146–5150.
[19] Z. Hua, L. Salamanca-Riba, M. Wuttig, P.K. Soltani, J. Opt. Soc. Am. B 10 (1993) 4164–4169.